analytical chemistry

Article

pubs.acs.org/ac

Enhanced Photoelectrochemical Strategy for Ultrasensitive DNA Detection Based on Two Different Sizes of CdTe Quantum Dots Cosensitized TiO_2/CdS:Mn Hybrid Structure

Gao-Chao Fan,[†] Li Han,[†] Jian-Rong Zhang,*[,†,‡] and Jun-Jie Zhu*[,†]

[†]State Key Laboratory of Analytical Chemistry for Life Science, School of Chemistry and Chemical Engineering, Nanjing University, Nanjing 210093, People's Republic of China

[‡]School of Chemistry and Life Science, Nanjing University Jinling College, Nanjing 210089, People's Republic of China

Supporting Information

ABSTRACT: A TiO_2/CdS:Mn hybrid structure cosensitized with two different sizes of CdTe quantum dots (QDs) was designed to develop a novel and ultrasensitive photoelectrochemical DNA assay. In this protocol, TiO_2/CdS:Mn hybrid structure was prepared by successive adsorption and reaction of Cd^{2+}/Mn^{2+} and S^{2-} ions on the surface of TiO_2 film and then was employed as matrix for immobilization of hairpin DNA probe, whereas large-sized CdTe−COOH QDs and small-sized CdTe−NH_2 QDs as signal amplification elements were successively labeled on the terminal of hairpin DNA probe. The target DNA detection was based upon the photocurrent change originated from conformation change of the hairpin DNA probe after hybridization with target DNA. In the absence of target DNA, the immobilized DNA probe was in the hairpin form and the anchored different sizes of CdTe−COOH and CdTe−NH_2 QDs were close to the TiO_2/CdS:Mn electrode surface, which led to a very strong photocurrent intensity because of the formation of the cosensitized structure. However, in the presence of target DNA, the hairpin DNA probe hybridized with target DNA and changed into a more rigid, rodlike double helix, which forced the multianchored CdTe QDs away from the TiO_2/CdS:Mn electrode surface, resulting in significantly decreased photocurrent intensity because of the vanished cosensitization effect. By using this cosensitization signal amplification strategy, the proposed DNA assay could offer an ultrasensitive and specific detection of DNA down to 27 aM, and it opened up a new promising platform to detect various DNA targets at ultralow levels for early diagnoses of different diseases.

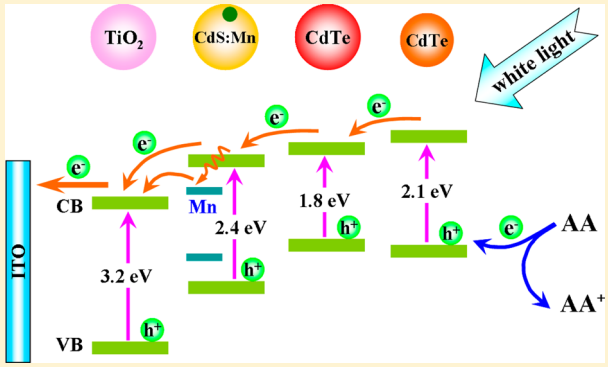

Detection of specific DNA sequences has attracted great research interest due to its broad applications in molecular diagnostics,[1,2] genetics therapy,[3] environmental monitoring,[4] forensic analysis,[5] early screening of cancers,[6] etc. Commonly, detection of DNA sequences is mainly based upon DNA hybridization. In order to read out the DNA hybridization events, different kinds of markers such as fluorescent molecules, luminescent materials, electrochemical species, enzymes, and photoelectric materials were used as transducer elements labeling on the target DNA or DNA probe. Consequently, various methods, for instance, colorimetric,[7] piezoelectric,[8] fluorescence,[9] chemiluminescence,[10] electrochemical,[11,12] and electrochemiluminescence,[13,14] have been developed for DNA detection. Despite many advances of these DNA assays, some of them relate to drawbacks such as limited sensitivity, complicated equipment, and relatively expensive and time-consuming detection. As the DNA concentration is often at a very low level in biological samples, it is very necessary to explore ultrasensitive, selective, simple, and inexpensive method for detecting specific DNA sequences.

Photoelectrochemical detection is a newly appeared yet vibrantly developing analytical method for rapid and high-throughput biological assays.[15] Benefiting from the different energy forms of excitation source (light) and detection signal (current), photoelectrochemical detection possesses potentially high sensitivity due to the reduced background signals.[16] Besides, advantageously inherited from the electrochemical method, the photoelectrochemical instrument is simple, portable, and inexpensive compared with conventional optical methods.[17] Of course, photoactive material plays a major role in the performances of the photoelectrochemical biosensor. For highly sensitive detection, the photoelectrochemical sensing system with enhanced photocurrent intensity and less electron−hole recombination is desirable. To achieve this target, a cosensitized structure, which is composed of the basic photoactive material and two or more sensitizers, is very promising. Generally, different semiconductors have different band gaps, causing their different optimal absorption ranges. As a result, coupling of small band gap semiconductors with large

Received: August 15, 2014
Accepted: October 8, 2014
Published: October 8, 2014

Scheme 1. Construction Process of the Photoelectrochemical DNA Assay

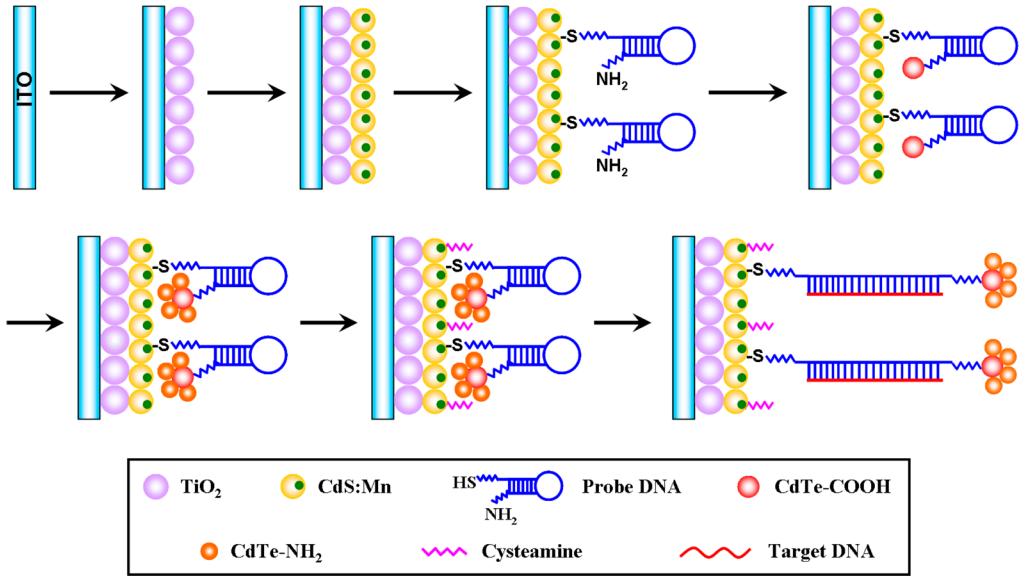

band gap ones to obtain a cosensitized structure with cascade band-edge levels can not only enhance the utilization of light energy but also facilitate charge separation, and therefore promote the photo-to-current conversion efficiency.[18] For example, Lee and Lo[19] reported that the TiO_2/CdSe or TiO_2/CdS photoelectrode only reached 1.24% or 1.15% conversion efficiency under one sun illumination, whereas TiO_2/CdS/CdSe photoelectrode (in which TiO_2 served as the basic photoactive material; CdS and CdSe served as two sensitizers) could achieve a conversion efficiency of 2.90%, which was more than twice that of a TiO_2/CdSe or TiO_2/CdS photoelectrode. Accordingly, the cosensitization strategy can efficiently achieve signal amplification. To date, numerous semiconductor nanomaterials such as ZnO,[20] TiO_2,[21] CdSe,[22] CdS,[23] CdTe,[24] and Bi_2S_3[25] have been used for fabricating various photoelectrochemical biosensors, yet very few works focused on the cosensitization strategy to enhance the sensitivity of the biosensors. For sensitive detection of DNA sequences, polymerase chain reaction (PCR),[9,26] rolling circle amplification (RCA),[27,28] and hybridization chain reaction (HCR)[2,29] represent the most widely used signal amplification strategies with powerful amplification capabilities. However, these approaches are relatively sophisticated, expensive, and time-consuming because of the introduction of auxiliary enzymes and other DNA fragments. In contrast, the cosensitization strategy only needs two or more semiconductor sensitizers to amplify the detection signals and can avoid these shortcomings. Thanks to the apparent advantages of significant signal amplification as well as saving time and cost, the cosensitization strategy would certainly be desirable. Unfortunately, to best of our knowledge, this superior signal amplification strategy has not been reported in photoelectrochemical DNA assay until now.

Herein, we present a novel photoelectrochemical DNA assay based on the cosensitization strategy for signal amplification, as illustrated in Scheme 1. Initially, TiO_2 nanoparticles were coated onto a bare indium−tin oxide (ITO) electrode and the compact film was formed after high-temperature sintering. Then, Mn-doped CdS (CdS:Mn) quantum dots (QDs) were assembled on the TiO_2 film by successive adsorption and reaction of Cd^{2+}/Mn^{2+} and S^{2-} ions to form a TiO_2/CdS:Mn hybrid structure, which acted as the photoelectrochemical matrix for the sensing electrode. Next, the hairpin DNA probes were firmly bound on the surface of CdS:Mn through a S−Cd bond. Subsequently, a large-sized CdTe−COOH QD as the first signal amplification element was labeled on the terminal of a hairpin DNA probe via the classic EDC coupling reaction between amino and carbonyl groups. Later, multiple small-sized CdTe−NH_2 QDs as the second signal amplification elements were connected on the surface of the previously anchored, large-sized CdTe−COOH QD also via the classic EDC coupling reaction. In this case, the photocurrent intensity of the sensing electrode significant enhanced due to the formation of the different sized CdTe QDs cosensitized TiO_2/CdS:Mn hybrid structure. After blocking unbound sites on the electrode surface with cysteamine, the target DNA was detected by the photocurrent decrease originated from the conformation change of the hairpin DNA probe after DNA hybridization which resulted in disappeared cosensitization effect. The designed DNA bioassay exhibited ultrahigh sensitivity, selectivity, and reproducibility. The proposed cosensitization signal amplification strategy also provided a general consideration for the design of the photoelectrochemical DNA biosensors to detect other DNA sequences.

EXPERIMENTAL SECTION

Materials and Reagents. ITO slices (type JH52, ITO coating 30 ± 5 nm, sheet resistance ≤10 Ω/square) were ordered from Nanjing Zhongjingkeyi Technology Co., Ltd. (China). Cadmium nitrate ($Cd(NO_3)_2{\cdot}4H_2O$) was obtained from Shanghai Jinshan Tingxin Chemical Plant (China). Sodium sulfide ($Na_2S{\cdot}9H_2O$), manganese acetate ($Mn(Ac)_2{\cdot}4H_2O$), and methanol were obtained from Nanjing Chemical Reagent Co., Ltd. (China). TiO_2 powder (P25) was purchased from the Degussa Co. (Germany). Cadmium chloride ($CdCl_2{\cdot}2.5H_2O$) and sodium hydroxide (NaOH) were purchased from Shanghai Chemical Reagent Co. (China). Sodium tellurite (Na_2TeO_3), sodium borohydride ($NaBH_4$), 3-mercaptopropionic acid (MPA), cysteamine (CA), 1-ethyl-3-(3-(dimethylamino)propyl) carbodiimide hydrochloride (EDC),

dx.doi.org/10.1021/ac503043w | Anal. Chem. 2014, 86, 10877−10884

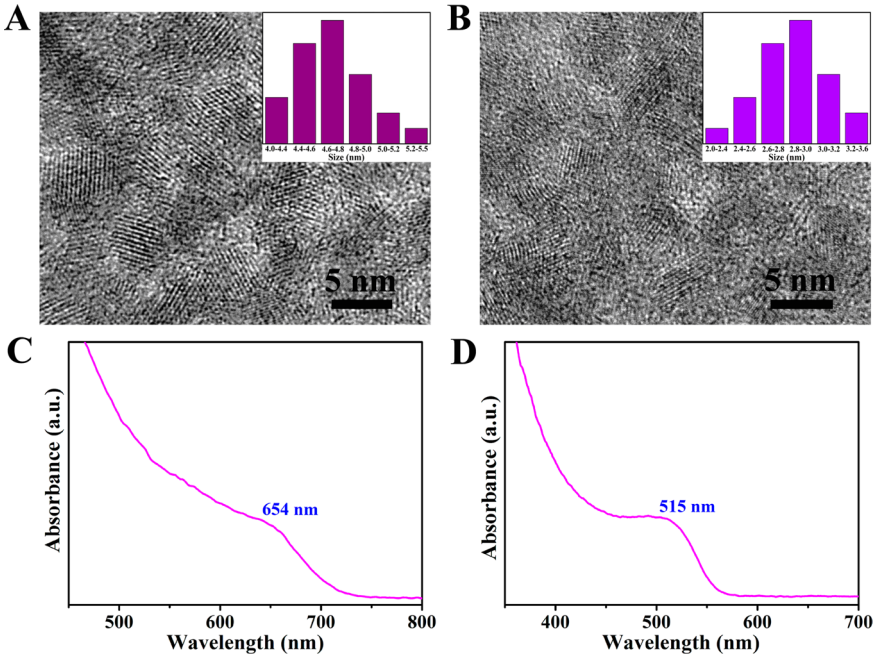

Figure 1. HRTEM images of the (A) CdTe−COOH and (B) CdTe−NH_2 QDs; UV−vis absorption spectra of the (C) CdTe−COOH and (D) CdTe−NH_2 QDs. Insets in parts A and B: size distribution of the QDs.

N-hydroxysuccinimide (NHS), and tris(2-carboxyethyl)-phosphine (TCEP) were all obtained from Sigma-Aldrich (U.S.A.). Ascorbic acid (AA) was purchased from Sinopharm Chemical Reagent Co., Ltd. (China). All other reagents were of analytical grade and used as received. All aqueous solutions were prepared with deionized water (DI water, 18 MΩ/cm), which was obtained from a Milli-Q water purification system. Tris−HCl buffer solution (pH 7.4, 10 mM) containing 0.1 M NaCl was used for preparation and hybridization of DNA stock solutions.

The oligonucleotides used in this work were ordered from Shenggong Bioengineering Co., Ltd. (Shanghai, China) with the following sequences: hairpin DNA probe, 5′-H_2N−-$(CH_2)_6$−CTC GCT TGG AAT AGC TGT GAT CAT TGT TAT TAG CGA GTT T−$(CH_2)_6$−SH-3′; target DNA, 5′-CTC GCT AAT AAC AAT GAT CAC AGC TAT TCC A-3′; single-base mismatch, 5′-CTC GCT AAT AAC AAT TAT CAC AGC TAT TCC A-3′; noncomplementary, 5′-TAT ATC TGA TCT GTC CCA ATT GTA CGA GTA T-3′.

Apparatus. A 500 W Xe lamp was used as the irradiation source with the light intensity of 400 $\mu W \cdot cm^{-2}$ estimated by a radiometer (Photoelectric Instrument Factory of Beijing Normal University). Photocurrent was measured on a CHI 660D electrochemical workstation (Shanghai Chenhua Apparatus Corporation, China) with a three-electrode system: a 0.25 cm^2 modified ITO as working electrode, a Pt wire as counter electrode, and a saturated Ag/AgCl electrode as reference electrode. The UV−visible (UV−vis) absorption spectra were tested on a UV-3600 UV−vis spectrophotometer (Shimadzu, Japan). Electrochemical impedance spectroscopy (EIS) was performed on an Autolab potentiostat/galvanostat (PGSTAT 30, Eco Chemie B.V., Utrecht, Netherlands) with a three-electrode system in 0.1 M KCl solution containing 5.0 mM $K_3[Fe(CN)_6]/K_4[Fe(CN)_6]$ (1:1) mixture as a redox probe and recorded in the frequency range of 0.01 Hz to 100 kHz with an amplitude of 50 mV. Transmission electron microscopy (TEM) was performed with a JEOL-2100 transmission electron microscope (JEOL, Japan).

Synthesis of CdTe−COOH and CdTe−NH_2 QDs. The synthetic procedures of water-soluble CdTe−COOH QDs and CdTe−NH_2 QDs were based on the literature methods with appropriate modifications (see the Supporting Information).[30,31]

Preparation of the ITO/TiO_2/CdS:Mn Electrode. Prior to use, ITO slices were cleaned by ultrasonic treatment for 15 min in acetone, 1 M NaOH of water/ethanol mixture (1:1, v/v), and water, respectively, and then dried at 90 °C for 12 h. Next, 6 mg of TiO_2 powder was ultrasonically dispersed in 6 mL of DI water, and then 20 μL of this homogeneous suspension (1.0 mg/mL) was dropped onto a piece of ITO slice with fixed area of 0.25 cm^2. After air drying, the film was sintered at 450 °C for 30 min in air atmosphere and then cooled down to the room temperature. The deposition of CdS:Mn on the ITO/TiO_2 electrode was according to the successive ionic layer adsorption and reaction (SILAR) method with some modifications.[32] The ITO/TiO_2 electrode was first dipped into 0.1 M $Cd(NO_3)_2$ mixed with 0.08 M $Mn(Ac)_2$ methanol solution for 1 min and rinsed with methanol, then followed by dipping into 0.1 M Na_2S methanol/water mixture (1:1, v/v) for 1 min, and again rinsed with methanol. This SILAR cycle was repeated twice, and the ITO/TiO_2/CdS:Mn electrode was acquired.

Fabrication of the Biosensor and DNA Analysis. Briefly, 20 μL of 2.5 μM hairpin DNA probe pretreated by TCEP (0.6 μL, 10 mM) for 1 h was dropped on the ITO/TiO_2/CdS:Mn electrode, and it was allowed to incubate at 4 °C for 12 h. After being rinsed with Tris−HCl buffer (10 mM, pH 7.4) to remove the unbound hairpin DNA probe, the electrode was covered with 20 μL of CdTe−COOH QDs containing 20 mM EDC and 10 mM NHS for 1 h at room temperature, and then washed with Tris−HCl buffer. Next, 20 μL of CdTe−NH_2 QDs was dropped on the electrode and incubated at room temperature for 2 h, which allowed CdTe−NH_2 QDs to react with previously activated CdTe−COOH QDs on the electrode

dx.doi.org/10.1021/ac503043w | *Anal. Chem.* 2014, 86, 10877−10884

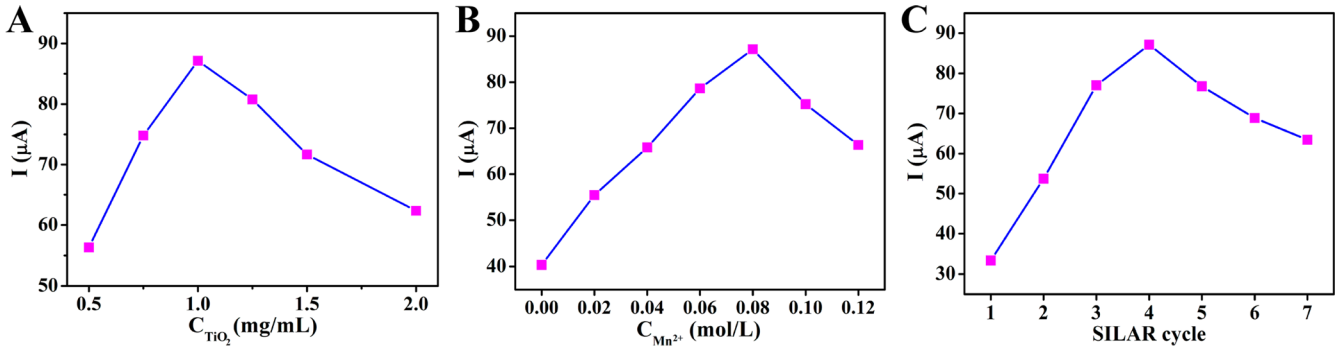

Figure 2. Effects of (A) concentration of TiO_2 suspension, (B) concentration of Mn^{2+}, and (C) coating number of CdS:Mn on photocurrent responses of the ITO/TiO_2/CdS:Mn electrode.

surface. Subsequently, the electrode was rinsed with Tris−HCl buffer and then incubated with 20 μL of 1 mM CA at room temperature for 1 h to block nonspecific binding sites. After being rinsed with Tris−HCl buffer, the resulting electrode was employed as a photoelectrochemical DNA biosensor and incubated with 20 μL of different concentrations of target DNA at 37 °C for 2 h. Finally, the electrode was rinsed with Tris−HCl buffer and prepared for photoelectrochemical detection.

Photoelectrochemical Measurement. Photoelectrochemical detection was carried out at room temperature in Tris−HCl buffer (0.1 M, pH 7.4) containing 0.1 M AA, which was served as a sacrificial electron donor during the photocurrent measurement. White light, with a spectral range of 200−2500 nm, was utilized as excitation light and was switched on and off every 10 s. The applied potential was 0.0 V. The AA electrolyte was deaerated by pure nitrogen for 10 min before photocurrent measurement.

RESULTS AND DISCUSSION

Characterization of CdTe−COOH and CdTe−NH_2 QDs. Parts A and B of Figure 1 show the high-resolution TEM (HRTEM) images of the prepared CdTe−COOH and CdTe−NH_2 QDs, respectively. The lattice fringes of the two kinds of QDs are clearly observed, and the average sizes of 4.68 and 2.85 nm were obtained from their size distribution. Parts C and D of Figure 1 display the UV−vis absorption spectra of the prepared CdTe−COOH and CdTe−NH_2 QDs, respectively. For CdTe−COOH QDs, the spectrum exhibited a broad absorption range below 735 nm and an evident absorption peak located at 654 nm, whereas the spectrum of CdTe−NH_2 QDs exhibited an absorption range below 580 nm and an obvious absorption peak located at 515 nm. According to Peng's empirical formula derived from UV−vis absorption,[33] the sizes of CdTe−COOH and CdTe−NH_2 QDs were calculated to be 4.43 and 2.71 nm, respectively. The band gap values of the prepared CdTe−COOH and CdTe−NH_2 QDs could also be acquired from UV−vis absorption spectra based on the following equation:[34]

$$\alpha h\nu = A(h\nu - E_g)^{1/2} \quad (1)$$

where α, h, ν, E_g, and A represent the absorption coefficient, Planck constant, light frequency, band gap, and constant, respectively. According to eq 1, the plot of $(\alpha h\nu)^2$ versus $h\nu$ was first obtained. Then, by extrapolating the fitting straight line of the plot to $a = 0$, the band gap E_g was acquired. Thus, for the as-prepared CdTe−COOH and CdTe−NH_2 QDs, the band gap values were estimated to be 1.8 and 2.1 eV, respectively.

Photoelectrochemical Property of the ITO/TiO_2/CdS:Mn Electrode. TiO_2 is a wide energy band gap (~3.2 eV) semiconductor material, which can only absorb the ultraviolet light (<387 nm). CdS has a narrower energy band gap (~2.4 eV), and its absorption range can reach to the wavelength of 550 nm. Thus, coupling of CdS with TiO_2 to form a TiO_2/CdS hybrid structure can evidently extend the absorption range, increase the utilization of light energy, and promote the photocurrent intensity.[35] In order to improve electron−hole recombination and further enhance the photocurrent intensity, Mn^{2+} can be introduced into CdS to form Mn-doped CdS (CdS:Mn), because the lifetime of electron−hole recombination for CdS:Mn is up to hundreds of microseconds, which is much longer than that of dozens of nanoseconds for CdS.[36] Thus, herein, a TiO_2/CdS:Mn hybrid structure was first employed as the matrix for photoelectrochemical sensing electrode. As the thickness of TiO_2 film, the content of doped Mn^{2+} in CdS, and the deposition of CdS:Mn could influence the photocurrent intensity of ITO/TiO_2/CdS:Mn electrode, the optimal preparation conditions should be investigated.

Since the area of the ITO electrode (0.25 cm^2) and the applied volume of the TiO_2 suspension (20 μL) were fixed, the thickness of TiO_2 film could be adjusted by the concentration of TiO_2 suspension. Figure 2A shows the photocurrent intensity of the ITO/TiO_2/CdS:Mn electrode prepared with different concentrations of TiO_2 suspensions, and with 0.08 M Mn^{2+} and four SILAR cycles of CdS:Mn fixed. It could been seen that the ITO/TiO_2/CdS:Mn electrode fabricated with 1.0 mg/mL suspension exhibited the highest photocurrent intensity. Increasing the concentration of TiO_2 suspension could offer more amount of TiO_2, which enlarged the surface area of TiO_2 film to absorb more amount of CdS:Mn. As a result, more light absorption occurred on the ITO/TiO_2/CdS:Mn electrode and the photocurrent intensity increased. However, with further increasing the concentration of TiO_2 suspension, the diffusion resistance for electron motion in thicker TiO_2 film evidently increased due to more and more surface recombination centers on excessive TiO_2,[37] leading to the gradually decreased photocurrent intensity. Thus, 1.0 mg/mL TiO_2 suspension was adopted for fabricating the electrode.

The doping content of Mn^{2+} in CdS could be adjusted by the concentration of Mn^{2+} during the SILAR process.[32] Figure 2B exhibits the photocurrent intensity of the ITO/TiO_2/CdS:Mn electrode prepared with different concentrations of Mn^{2+}, and

dx.doi.org/10.1021/ac503043w | Anal. Chem. 2014, 86, 10877−10884

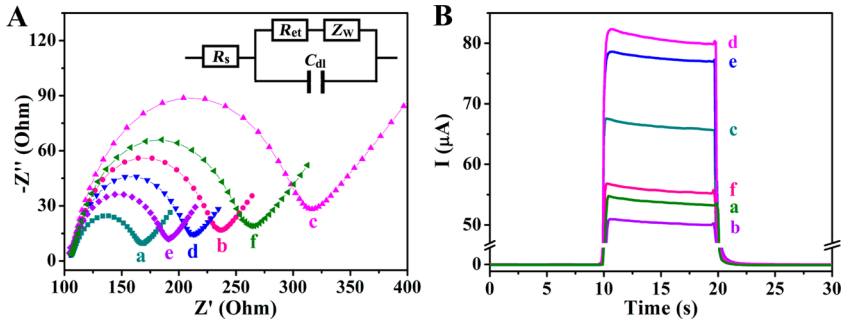

Figure 3. (A) EIS and (B) photocurrent response of (a) the ITO/TiO_2/CdS:Mn electrode, (b) after hairpin DNA probe immobilization, (c) after anchoring CdTe−COOH QDs, (d) after further linking with CdTe−NH_2 QDs, (e) after CA blocking, and (f) after incubation with 20 μL of 1 μM target DNA. Inset of part A: the electrical equivalent circuit applied to fit the impedance spectra; R_s, Z_w, R_{et}, and C_{dl} represent ohmic resistance of the electrolyte, Warburg impedance, electron-transfer resistance, and the double layer capacitance, respectively.

with 1.0 mg/mL TiO_2 suspension and four SILAR cycles of CdS:Mn fixed. Along with increase of the concentration of Mn^{2+}, the doping content of Mn^{2+} in CdS increased, promoting the formation of more midgap centers. Accordingly, the charge separation was significantly improved and the photocurrent intensity increased. It could be seen that the ITO/TiO_2/CdS:Mn electrode fabricated by using 0.08 M Mn^{2+} possessed the highest photocurrent intensity. After the concentration of Mn^{2+} further increased, more and more excitation electrons were trapped by excessive amount of Mn−Mn ion pairs,[38] leading to gradually decreased photocurrent intensity. Thus, 0.08 M Mn^{2+} was used in the SILAR process to fabricate the electrode.

The deposition of CdS:Mn could be adjusted by SILAR cycles. Figure 2C shows the photocurrent intensity of ITO/TiO_2/CdS:Mn electrodes prepared with different SILAR cycles of CdS:Mn, and with 1.0 mg/mL TiO_2 suspension and 0.08 M doped Mn^{2+} fixed. As the SILAR cycle increased, the deposition of CdS:Mn gradually accumulated, resulting in more and more light absorption, and the photocurrent intensity increased. As could be seen, the ITO/TiO_2/CdS:Mn electrode with four SILAR cycles of CdS:Mn reached the highest photocurrent intensity. After the SILAR cycle further increased, the excessive amount of CdS:Mn offered more and more surface recombination centers which evidently increased the diffusion resistance for electron motion, and therefore, the photocurrent intensity gradually decreased.[39] According to the previous work by Santra and Kamat,[32] the absorption range of CdS:Mn was below 570 nm, which partly overlapped with that of the two layers of subsequently labeled CdTe−COOH (<735 nm) and CdTe−NH_2 QDs (<580 nm). In order to achieve optimal signal amplification, two SILAR cycles of CdS:Mn was chosen to fabricate the electrode.

EIS Characterization of the DNA Sensor Construction. As an effective technique for characterizing the interface properties of electrodes, EIS was employed to monitor the fabrication process of the DNA biosensor. Figure 3A shows the impedance spectra of the electrodes involved in different fabrication steps, and its inset is the corresponding equivalent circuit. The impedance spectra include a semicircle at higher frequencies representing the electron-transfer-limited process and a linear part at lower frequencies resulting from the diffusion-limited process. The semicircle diameter equals the electron-transfer resistance (R_{et}), which reflects the restricted diffusion of the redox probe accessing the layer. And the R_{et} values can be obtained from fitted results with the equivalent circuit. For the ITO/TiO_2/CdS:Mn electrode, the impedance spectrum exhibited a relatively small semicircle (Figure 3A, curve a, R_{et} = 62 Ω). After hairpin DNA probe and CdTe−COOH QDs were immobilized onto the surface of the ITO/TiO_2/CdS:Mn electrode step by step, gradually increased R_{et} was observed due to the low conductivity of DNA or semiconductors (Figure 3A, curve b, R_{et} = 129 Ω; curve c, R_{et} = 208 Ω). It was worth noting that the increment of R_{et} for hairpin DNA probe modification (ΔR_{et} = 67 Ω) was less than that of CdTe−COOH QDs modification (ΔR_{et} = 79 Ω), which was because amino groups of hairpin DNA generated a positively charged surface that improved the ability of the negatively charged redox probe ($[Fe(CN)_6]^{3-}/[Fe(CN)_6]^{4-}$) to access the electrode surface, whereas carboxyl groups of CdTe−COOH QDs generated a negatively charged surface that reduced the ability of the redox probe to access the electrode surface. Subsequently, CdTe−NH_2 QDs were covalently bound on the electrode, and the R_{et} (Figure 3A, curve d, R_{et} = 106 Ω) significantly decreased to less than that of Figure 3A, curve b. It was because each large-sized CdTe−COOH QD had linked with multiple small-sized CdTe−NH_2 QDs resulting in the excess of amino groups than carboxyl groups, which evidently improved the ability of the redox probe to access the electrode surface. After the electrode was blocked with CA, the R_{et} further decreased (Figure 3A, curve e, R_{et} = 87 Ω) because of the terminal amino group on CA. While the as-obtained sensing electrode was incubated with target DNA, the R_{et} evidently increased (Figure 3A, curve f, R_{et} = 158 Ω), indicating that the target DNA had hybridized with hairpin DNA probe. Thus, the EIS characterization suggested that the proposed DNA biosensor was successfully fabricated.

Cosensitization Effect for Signal Amplification. To achieve ultrasensitive DNA detection, a cosensitization strategy for signal amplification was applied. In order to acquire a cascade cosensitized structure, traditionally, different semiconductor materials need to be meticulously selected. As photosensitizers, semiconductor quantum dots not only exhibit the merits of high absorption coefficient, delivery of hot electrons, and generation of multiple electron carriers, but also possess the unique property of tunability of the band gap via varying particle size.[40−43] We hereby first used the same semiconductor quantum dots with different sizes as different sensitizers to develop a new cosensitized structure for the design of an ultrasensitive DNA assay, and the electron-transfer mechanism is shown in Scheme 2. In this DNA assay, the TiO_2/CdS:Mn hybrid structure acted as photoelectrochemical matrix for the sensing electrode, whereas large-sized CdTe−COOH QDs and small-sized CdTe−NH_2 QDs, respectively,

dx.doi.org/10.1021/ac503043w | Anal. Chem. 2014, 86, 10877−10884

Scheme 2. Electron-Transfer Mechanism of the Designed DNA Biosensor in AA Electrolyte[a]

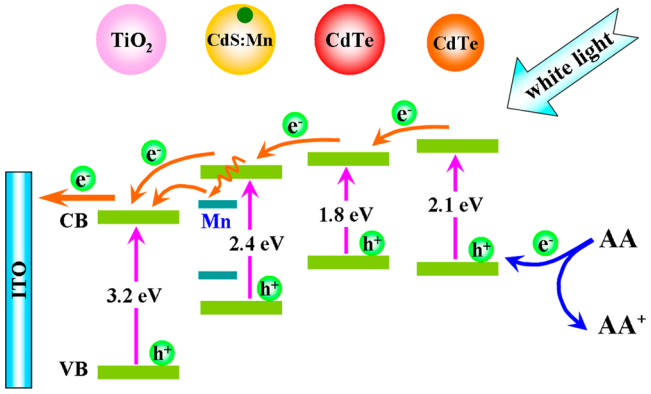

[a]The energy levels of the conduction band (CB) and valence band (VB) for TiO_2, CdS, and CdTe originated from the literatures (refs 44−46).

acted as the first and second signal amplification elements. Because of wave function confinement of the quantum dot, the band gap will increase with particle size decrease, leading to the conduction band of small-sized CdTe−NH_2 QDs being higher than that of CdTe−COOH QDs.[44] As one hairpin DNA probe possesses only one binding site, multilabeling of hairpin DNA probe with different sized CdTe QDs was adopted to achieve cosensitization signal amplification. After large-sized CdTe−COOH QDs were covalently bound with hairpin DNA probes, the photocurrent intensity evidently increased. It was because the absorbance range of the TiO_2/CdS:Mn hybrid structure was below the wavelength of 570 nm, whereas the CdTe−COOH QDs extended to 735 nm, which dramatically promoted the long-wavelength light harvest. When multiple small-sized CdTe−NH_2 QDs with the absorbance range below 580 nm were subsequently bound on the surface of the large-sized CdTe−COOH QDs, the photocurrent intensity further evidently increased, as the introduction of the CdTe−NH_2 QDs obviously increased the absorption efficiency of middle-wavelength light. Besides, Mn-doped CdS could also assist the cosensitization effect of these multianchored CdTe QDs to promote the photocurrent intensity, because Mn^{2+} created electronic states in the midgap region of CdS, which significantly reduced the electron recombination of photogenerated electrons coming from CdTe−COOH and CdTe−NH_2 QDs.[32] However, after being hybridized with target DNA, the hairpin DNA probe changed from the hairpin shape to a more rigid, rodlike double helix, and the multianchored CdTe QDs on the terminal of hairpin DNA probe were far away from the TiO_2/CdS:Mn electrode surface, which resulted in vanished cosensitization effect of the CdTe QDs to TiO_2/CdS:Mn. Thus, based on conformation change of hairpin DNA probe, the target DNA could be sensitively detected by using this cosensitization signal amplification strategy.

In order to verify the feasibility of the designed cosensitization strategy for signal amplification, photocurrent characterization of the prepared DNA biosensor was carried out, as shown in Figure 3B. The ITO/TiO_2/CdS:Mn electrode exhibited an evident photocurrent response (Figure 3B, curve a, I = 53.74 μA). After hairpin DNA probe immobilization, the photocurrent decreased moderately (Figure 3B, curve b, I = 50.35 μA), which could be attributed to the relatively weak charge transfer of the DNA sequence. After further anchoring CdTe−COOH and CdTe−NH_2 QDs to the terminal of hairpin DNA probe successively, the photocurrent intensity significantly increased (Figure 3B, curve c, I = 66.15 μA; curve d, I = 80.61 μA), demonstrating that the cosensitization effect of these CdTe QDs was very effective. After CA blocking, the photocurrent intensity decreased slightly (Figure 3B, curve e, I = 78.56 μA), because immobilization of the small organic molecule of CA partly obstructed AA to the electrode surface for reaction with the photogenerated holes. After the sensing electrode was incubated with target DNA, the photocurrent decreased significantly (Figure 3B, curve f, I = 55.58 μA) and almost returned to the initial value of the ITO/TiO_2/CdS:Mn electrode, which indicated that the cosensitization effect of these CdTe QDs vanished. Accordingly, photocurrent characterization proved that the cosensitization signal amplification strategy for target DNA detection was achieved.

Photoelectrochemical Detection for Target DNA. The cosensitization signal amplification for photoelectrochemical DNA detection was based upon the conformation change of hairpin DNA probe after hybridization with target DNA. The photocurrent response was directly related to the concentration of target DNA. Figure 4A exhibits the photocurrent responses of the designed DNA biosensor after incubation with different concentrations of target DNA. As the cosensitization effect would disappear after DNA hybridization, the photocurrent gradually decreased with increasing the concentration of target DNA. As shown in Figure 4B, the photocurrent response linearly decreased with increase of logarithm of target DNA concentration in the range from 50 aM to 50 pM. The regression equation was I = 62.27 − 3.11 log C (pM), with the correlation coefficient of 0.9968. The detection limit (S/N = 3)

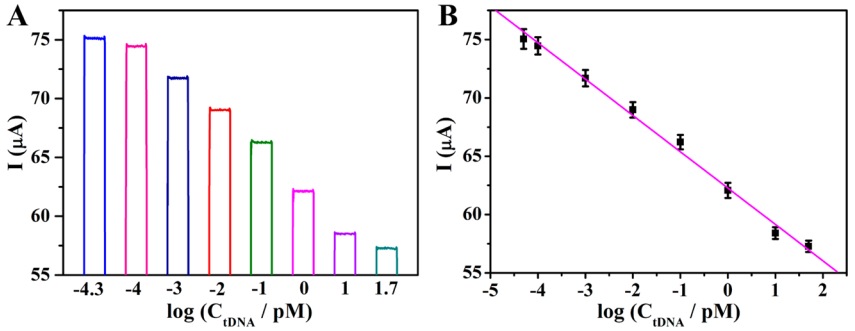

Figure 4. (A) Photocurrent response and (B) calibration curve of the DNA biosensor for detection of different concentrations of target DNA. The error bars showed the standard deviation of five replicate determinations.

dx.doi.org/10.1021/ac503043w | Anal. Chem. 2014, 86, 10877−10884

for target DNA concentration was estimated to be 27 aM. To illustrate the sensitivity, we compared the designed DNA bioassay not only with previously reported photoelectrochemical protocols but also with other assays, as shown in Supporting Information Table S1. It demonstrated that the well-designed photoelectrochemical DNA assay presented a much lower detection limit as well as a wider linear range.

Besides, to show excellent performance of the cosensitization signal amplification, the DNA bioassay with single-sensitization effect was constructed and tested. As illustrated in Supporting Information Scheme S1, the sensor construction was similar as the cosensitization strategy only with the second signal amplification elements removed. The photoelectrochemical testing results (see Supporting Information Figure S1) revealed that the single-sensitization signal amplification for target DNA detection exhibited a detection limit of 0.64 fM, which was nearly 24 times higher than that of the cosensitization signal amplification. Thus, the control experiment also proved an obvious superiority of the cosensitization signal amplification strategy.

Selectivity and Reproducibility of the DNA Assay. The selectivity of the designed DNA assay was investigated by comparing the photocurrent response to different DNA sequences, including target DNA, single-base mismatch DNA, and noncomplementary DNA at the same concentration of 10 pM, respectively. As shown in Figure 5, the photocurrent

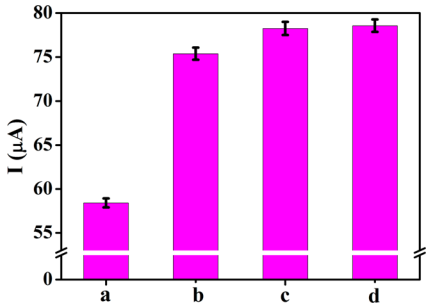

Figure 5. Photocurrent responses of the DNA biosensor incubated in 20 μL of 10 pM different DNA sequences: (a) target DNA, (b) single-base mismatch DNA, (c) noncomplementary DNA, and (d) blank. The error bars showed the standard deviation of five replicate determinations.

response of target DNA exhibited a significant decrease than that of the blank test (ΔI = 20.15 μA). Although the photocurrent decrease of single-base mismatch DNA was also observed (ΔI = 3.18 μA), it was not comparable with that of the target DNA. Meanwhile, the photocurrent response of noncomplementary DNA was very close to that of the blank test. These results demonstrated that the photocurrent response was specifically triggered by the conformation change of hairpin DNA probe after hybridization with target DNA, which indicated that the proposed DNA assay could offer high specificity.

The reproducibility of the proposed DNA assay was evaluated by analyzing five independently fabricated sensing electrodes. The photocurrent response offered a relative standard deviation (RSD) of 4.6% toward 10 fM target DNA, which indicated an acceptable precision and reproducibility of this bioassay.

CONCLUSIONS

In summary, we presented a novel photoelectrochemical platform for ultrasensitive detection of DNA based on a cosensitization strategy. Multilabeling of hairpin DNA probe with different sized CdTe QDs was adopted to achieve a cosensitization effect to significantly amplify the photocurrent signal. Conformation change of hairpin DNA probe after hybridization with target DNA promoted the disappearance of the cosensitization effect to sensitively decrease the photocurrent signal. Due to excellent photoelectrochemical performance of this cosensitization effect, the well-designed DNA assay could offer an ultralow detection limit of 27 aM and a wide linear range from 50 aM to 50 pM for target DNA detection. Benefiting from its simplicity, sensitivity, specificity, and reproducibility, the proposed photoelectrochemical platform shows great promise for the detection of trace levels of DNA and has a wide potential application in bioanalysis.

ASSOCIATED CONTENT

Supporting Information

Additional information as noted in text. This material is available free of charge via the Internet at http://pubs.acs.org.

AUTHOR INFORMATION

Corresponding Authors

*E-mail: jrzhang@nju.edu.cn. Phone/Fax: +86 25 83686130.
*E-mail: jjzhu@nju.edu.cn. Phone/Fax: +86 25 83597204.

Notes

The authors declare no competing financial interest.

ACKNOWLEDGMENTS

We gratefully appreciate the National Natural Science Foundation (21375059, 21175065, 21335004, and 21121091) and the National Basic Research Program (2011CB933502) of China.

REFERENCES

(1) Dong, H. F.; Gao, W. C.; Yan, F.; Ji, H. X.; Ju, H. X. *Anal. Chem.* **2010**, *82*, 5511−5517.
(2) Huang, J.; Wu, Y.; Chen, Y.; Zhu, Z.; Yang, X.; Yang, C. J.; Wang, K.; Tan, W. *Angew. Chem., Int. Ed.* **2011**, *50*, 401−404.
(3) Huang, Y.; Zhang, Y. L.; Xu, X. M.; Jiang, J. H.; Shen, G. L.; Yu, R. Q. *J. Am. Chem. Soc.* **2009**, *131*, 2478−2480.
(4) Rodriguez-Mozaz, S.; Alda, M. J. L.; Barcelo, D. *Anal. Bioanal. Chem.* **2006**, *386*, 1025−1041.
(5) Carey, L.; Mitnik, L. *Electrophoresis* **2002**, *23*, 1386−1397.
(6) Bi, S.; Zhang, J. L.; Zhang, S. S. *Chem. Commun.* **2010**, *46*, 5509−5511.
(7) Sato, K.; Hosokawa, K.; Maeda, M. *J. Am. Chem. Soc.* **2003**, *125*, 8102−8103.
(8) Nie, L. B.; Yang, Y.; Li, S.; He, N. Y. *Nanotechnology* **2007**, *18*, 305501.
(9) Du, Y. Q.; Gao, P. F.; Wang, W.; Wang, T. T.; Chang, Y.; Wang, J.; Huang, C. Z. *Analyst* **2013**, *138*, 5745−5750.
(10) Zhang, S. S.; Zhong, H.; Ding, C. F. *Anal. Chem.* **2008**, *80*, 7206−7212.
(11) Zhang, Y.; Tang, Z.; Wang, J.; Wu, H.; Maham, A.; Lin, Y. *Anal. Chem.* **2010**, *82*, 6440−6446.
(12) Xu, J.; Wang, Q.; Xiang, Y.; Yuan, R.; Chai, Y. *Analyst* **2014**, *139*, 128−132.
(13) Shan, Y.; Xu, J. J.; Chen, H. Y. *Chem. Commun.* **2009**, 905−907.
(14) Zhou, H.; Zhang, Y. Y.; Liu, J.; Xu, J. J.; Chen, H. Y. *J. Phys. Chem. C* **2012**, *116*, 17773−17780.

(15) Wang, G. L.; Yu, P. P.; Xu, J. J.; Chen, H. Y. *J. Phys. Chem. C* **2009**, *113*, 11142−11148.
(16) Liang, M. M.; Liu, S. L.; Wei, M. Y.; Guo, L. H. *Anal. Chem.* **2006**, *78*, 621−623.
(17) Haddour, N.; Chauvin, J.; Gondran, C.; Cosnier, S. *J. Am. Chem. Soc.* **2006**, *128*, 9693−9698.
(18) Lee, Y. L.; Chi, C. F.; Liau, S. Y. *Chem. Mater.* **2010**, *22*, 922−927.
(19) Lee, Y. L.; Lo, Y. S. *Adv. Funct. Mater.* **2009**, *19*, 604−609.
(20) Tu, W. W.; Lei, J. P.; Wang, P.; Ju, H. X. *Chem.—Eur. J.* **2011**, *17*, 9440−9447.
(21) An, Y. R.; Tang, L. L.; Jiang, X. L.; Chen, H.; Yang, M. C.; Jin, L. T.; Zhang, S. P.; Wang, C. G.; Zhang, W. *Chem.—Eur. J.* **2010**, *16*, 14439−14446.
(22) Zhang, X. R.; Li, S. G.; Jin, X.; Li, X. M. *Biosens. Bioelectron.* **2011**, *26*, 3674−3678.
(23) Willner, I.; Patolsky, F.; Wasserman, J. *Angew. Chem., Int. Ed.* **2001**, *40*, 1861−1864.
(24) Wang, W. J.; Bao, L.; Lei, J. P.; Tu, W. W.; Ju, H. X. *Anal. Chim. Acta* **2012**, *744*, 33−38.
(25) Yin, H. S.; Sun, B.; Zhou, Y. L.; Wang, M.; Xu, Z. N.; Fu, Z. L.; Ai, S. Y. *Biosens. Bioelectron.* **2014**, *51*, 103−108.
(26) Cheglakov, Z.; Weizmann, Y.; Beissenhirtz, M. K.; Willner, I. *Chem. Commun.* **2006**, 3205−3207.
(27) Ji, H. X.; Yan, F.; Lei, J. P.; Ju, H. X. *Anal. Chem.* **2012**, *84*, 7166−7171.
(28) Long, Y.; Zhou, X. M.; Xing, D. *Biosens. Bioelectron.* **2013**, *46*, 102−107.
(29) Zhu, Z.; Lei, J. P.; Liu, L.; Ju, H. X. *Analyst* **2013**, *138*, 5995−6000.
(30) Zou, L.; Gu, Z. Y.; Zhang, N.; Zhang, Y. L.; Fang, Z.; Zhu, W. H.; Zhong, X. H. *J. Mater. Chem.* **2008**, *18*, 2807−2815.
(31) Wang, R. F.; Wang, Y. L.; Feng, Q. L.; Zhou, L. Y.; Gong, F. Z.; Lan, Y. W. *Mater. Lett.* **2012**, *66*, 261−263.
(32) Santra, P. K.; Kamat, P. V. *J. Am. Chem. Soc.* **2012**, *134*, 2508−2511.
(33) Yu, W. W.; Qu, L. H.; Guo, W. Z.; Peng, X. G. *Chem. Mater.* **2003**, *15*, 2854−2860.
(34) Yang, F.; Yan, N. N.; Huang, S.; Sun, Q.; Zhang, L. Z.; Yu, Y. *J. Phys. Chem. C* **2012**, *116*, 9078−9084.
(35) Wang, G. L.; Xu, J. J.; Chen, H. Y.; Fu, S. Z. *Biosens. Bioelectron.* **2009**, *25*, 791−796.
(36) Pradhan, N.; Sarma, D. D. *J. Phys. Chem. Lett.* **2011**, *2*, 2818−2826.
(37) Kuang, D. B.; Ito, S.; Wenger, B.; Klein, C.; Moser, J. E.; Humphry-Baker, R.; Zakeeruddin, S. M.; Gratzel, M. *J. Am. Chem. Soc.* **2006**, *128*, 4146−4154.
(38) Nag, A.; Chakraborty, S.; Sarma, D. D. *J. Am. Chem. Soc.* **2008**, *130*, 10605−10611.
(39) Vogel, R.; Hoyer, P.; Weller, H. *J. Phys. Chem.* **1994**, *98*, 3183−3188.
(40) Kongkanand, A.; Tvrdy, K.; Takechi, K.; Kuno, M.; Kamat, P. V. *J. Am. Chem. Soc.* **2008**, *130*, 4007−4015.
(41) Nozik, A. J. *Inorg. Chem.* **2005**, *44*, 6893−6899.
(42) Pandey, A.; Guyot-Sionnest, P. *J. Phys. Chem. Lett.* **2010**, *1*, 45−47.
(43) Beard, M. C. *J. Phys. Chem. Lett.* **2011**, *2*, 1282−1288.
(44) Ruhle, S.; Shalom, M.; Zaban, A. *ChemPhysChem* **2010**, *11*, 2290−2304.
(45) Grätzel, M. *Nature* **2001**, *414*, 338−344.
(46) Norris, D. J.; Efros, A. L.; Erwin, S. C. *Science* **2008**, *319*, 1776−1779.